Available online at www.sciencedirect.com

ScienceDirect

Advances in Space Research 73 (2024) 553–570

ADVANCES IN SPACE RESEARCH (a COSPAR publication)

www.elsevier.com/locate/asr

Investigating the contribution of BDS-3 observations to multi-GNSS single-frequency precise point positioning with different ionospheric models

Ahao Wang [a], Yize Zhang [b,*], Junping Chen [b,c], Hu Wang [d], Debao Yuan [a], Jinbao Jiang [a] Zehao Zhang [a]

[a] College of Geoscience and Surveying Engineering, China University of Mining and Technology-Beijing, Beijing 100083, China
[b] Shanghai Astronomical Observatory, Chinese Academy of Sciences, Shanghai 200030, China
[c] School of Astronomy and Space Science, University of Chinese Academy of Sciences, Beijing 100049, China
[d] Chinese Academy of Surveying & Mapping, Beijing 100036, China

Received 15 April 2023; received in revised form 10 October 2023; accepted 22 October 2023
Available online 29 October 2023

Abstract

Due to the advantages of low-cost and high precision, single-frequency precise point positioning (SF-PPP) plays a vital role in the booming market of the SF global navigation satellite system (GNSS) receivers. With the full completion of the BeiDou global navigation satellite system (BDS-3), its contribution to single-GNSS SF-PPP is worthy of comprehensive exploration. In this study, three SF-PPP models including ionosphere-corrected (IC), ionosphere-free (IF), and ionosphere-weighted (IW) strategies are analyzed, and four ionospheric models including the GPS Klobuchar, BDGIM (BeiDou global ionospheric delay correction model), CNES real-time VTEC (vertical total electron content) and GIM (global ionospheric maps) are used for conducting SF-PPP. As to GPS/GLONASS/Galileo-only IC SF-PPP, its 3D positioning accuracy can be improved by 6.9–11.6 % with the adoption of BDS-3 observations. Similarly, for the IF SF-PPP solution, the corresponding positioning accuracy and convergence time can be improved by at least 17.3 and 38.3 %, respectively. In IW SF-PPP, the convergence performance of the CNES-VTEC-constrained SF-PPP is much better than that of both GPS Klobuchar- and BDGIM-constrained solutions. When using the BDGIM constraints, the horizontal/vertical convergence time of GPS/Galileo + BDS-3 solutions can be shortened by at least 16.5/27.9 % in comparison with GPS/Galileo-only solutions. While for GIM-constrained SF-PPP, the convergence improvement is only shown in the vertical component. In summary, the GIM-constrained SF-PPP with quad-system observations has the best performance, compared to IF solution, its convergence time can be shortened by 82.8 % to 5.5 min in horizontal and 29.7 % to 26.0 min in vertical when converging to 0.3 m. Note that the corresponding improvements in the BDGIM-constrained solution are relatively limited with only 5 %. At present, the quad-system IW SF-PPP has the ability to achieve cm-level fast positioning, with an RMS of 0.06 m in horizontal, showing promising applications in engineering and scientific fields.

Keywords: BDS-3; Multi-GNSS; Single-frequency precise point positioning; Ionosphere-weighted; BDGIM

1. Introduction

In the booming global navigation satellite system (GNSS) market, the majority of smart devices, such as smartphones, fitness-tracking wristbands and shared

* Corresponding author.
E-mail address: zhyize@shao.ac.cn (Y. Zhang).

https://doi.org/10.1016/j.asr.2023.10.033
0273-1177/

bicycles, commonly use low-cost chipsets that only receive single-frequency (SF) GNSS signals. (Gill et al., 2017; Odolinski and Teunissen, 2018; Li et al., 2019; Wang et al., 2020b). Nowadays, the price of low-cost SF receivers can be as low as tens of dollars, and they are dozens or even hundreds of times lower than multi-frequency (MF) receivers. Thanks to the advances of multi-GNSS integrated processing, phase-smoothed code method, and ionospheric model, the SF precise point positioning (PPP) has the ability to provide dm- or even cm-level positioning accuracy. Therefore, the multi-GNSS SF-PPP has increasingly attracted the attention of low-cost GNSS users. With the full implementation of the BeiDou global navigation satellite system (BDS-3) since June 2020, most of the research related to BDS-3 mainly concentrated on the dual- or multi-frequency PPP, standard point positioning (SPP), and real-time kinematic (RTK) positioning technologies. There is little research on the SF-PPP, and the BDS-3 + GNSS solutions have not been evaluated (Shi et al., 2021; Wang et al., 2022b). Thus, the contribution of BDS-3 observations to single- or multi-GNSS SF-PPP with different processing scenarios needs to be comprehensively investigated using global monitoring stations. This work has been completed in this study.

Different from the DF or multi-frequency (MF) PPP where the ionospheric errors can be removed from ionosphere-free (IF) model, ionospheric delay as one of the largest errors in SF-PPP need to be handled properly. Nowadays, there are three widely used SF-PPP models including ionosphere-corrected (IC) model, ionosphere-free (IF) model and ionosphere-weighted (IW) model (Wang et al., 2020b). The IC model adopts undifferenced and uncombined code/phase observations, and the ionospheric error needs to be corrected by the existing ionospheric model. Hence the positioning results of the IC model are generally biased due to the inaccuracy of used ionospheric product (Ghoddousi-Fard and Lahaye, 2016; Wang et al., 2019). In this research, four types of ionospheric models, including Klobuchar (Klobuchar, 1987), the Center National d'Etudes spatiales (CNES) real-time VTEC (Vertical Total Electron Content) products (Nie et al., 2019; Wang et al., 2020a), global ionospheric maps (GIM) (Feltens, 2003; Hernández-Pajares et al., 2009), and BeiDou global broadcast ionospheric delay correction model (BDGIM) (Yuan et al., 2019), are applied to mitigate the ionospheric effects in IC-SF-PPP solution. To date, few literatures have been devoted to the comprehensive evaluation of BDGIM performance in the multi-GNSS IC-SF-PPP domain, thus some relevant results and findings can be presented through sufficient data processing of global monitoring stations in this study. With regard to IF model, namely the GRAPHIC (GRoup And PHase Ionospheric Correction) method (Montenbruck, 2003), the ionospheric errors can be completely eliminated by combining the code and phase observations at the same frequency. Although the IF model has the ability to carry out decimeter-level positioning, as the noise of GRAPHIC observation is magnified many times, its convergence time is normally long (Wang et al., 2020b; Chen et al., 2022).

In order to shorten the initialization time of multi-GNSS SF-PPP while ensuring high positioning accuracy, the external ionospheric-constrained IW model was proposed (Shi et al., 2012). This model not only uses raw code and phase observations with low noise, but also can totally remove the ionospheric effect by estimating the ionospheric parameters. Therefore, the IW model has the advantages of both IC and IF models (Wang et al., 2020b). As long as the external ionospheric model is accurate enough, the (re-) convergence of the IW model by applying a proper ionospheric constraint can be greatly improved (Li et al. 2019; Wang et al. 2022a). Some researchers have studied the influences of different ionospheric constraints on the performance of SF-PPP, especially on convergence. Compared with traditional IF model, the average convergence time of SF-PPP based on the Klobuchar-, NeQuick-, NTCM (Neustrelitz TEC Model)-, CNES-VTEC-, and GIM-constrained can be reduced by 11.2 % to 39.6 % (Su et al., 2019; Wang et al., 2019, 2020a, 2020b). However, there is no literature dedicated to investigating the contribution of BDGIM constraints to the performance of BDS-3/GNSS combined SF-PPP. In this study, sufficient BDGIM-constrained multi-GNSS SF-PPP tests were carried out to fill this gap.

In this contribution, the function model of IC, IF and IW BDS-3/GNSS combined SF-PPP is first introduced in detail. Then, the processing strategies and experimental datasets in positioning domain are described. Further, the performance of all adopted multi-GNSS SF-PPP models using different ionospheric corrections, especially for BDGIM model, are evaluated and compared. Some conclusions and findings are summarized in the end.

2. Methodology

On the basis of different ionospheric processing strategies, the algorithms of three BDS-3/GNSS combined SF-PPP including the IC, IF and IW models are introduced in detail.

2.1. Function model of the GNSS single-frequency PPP

The undifferenced and uncombined observation equations can be expressed as (Li et al., 2019; Wang et al., 2020b)

$$\begin{aligned} P^s_{i,k} &= \rho^s_k + dt_{r,k} - dt^s_k + T^s_k + \mu_i \cdot I^s_k + D_i - d^s_i + \varepsilon_{p_k} \\ L^s_{i,k} &= \rho^s_k + dt_{r,k} - dt^s_k + T^s_k - \mu_i \cdot I^s_k - N^s_i + B_i - b^s_i + \varepsilon_{L_k} \end{aligned} \tag{1}$$

where P and L denote the code and phase observations, respectively. s and r denote the satellite and receiver, respectively. i and k denote the frequency and epoch, respectively. ρ^s_k is the spatial geometric distance between the receiver and satellite antennas. dt^s_k is the satellite clock

offset; $dt_{r,k}$ is the receiver clock offset. T_k^s denotes the tropospheric error, I_k^s denotes the line-of-sight ionospheric error on the first frequency, and $\mu_i = \frac{f_1^2}{f_i^2}$ with f_i being the ith frequency. N_i^s is the integer ambiguity of the phase observation. D_i and B_i denote receiver hardware delays for code and phase observation, respectively, while d_i^s and b_i^s denote satellite hardware delays for code and phase observation, respectively. ε_{p_k} and ε_{L_k} are the observation noise for code and phase, respectively.

As to Eq. (1), the satellite clock offset dt_k^s can be fixed by precise products (e.g., GBM, WUM) from International GNSS Service (IGS) analysis centers (ACs). Since the precise satellite clocks are estimated by using IF observations, the given satellite clock offsets dt_{IF}^s incorporate the code hardware delays of different frequencies, which can be defined as

$$\begin{cases} dt_{IF}^{G/R/E} = dt^{G/R/E} + \frac{f_1^2}{f_1^2-f_2^2} d_1^{G/R/E} - \frac{f_2^2}{f_1^2-f_2^2} d_2^{G/R/E} \\ \quad = dt^{G/R/E} + d_1^{G/R/E} - \frac{f_2^2}{f_1^2-f_2^2} \mathrm{DCB}_{12}^{G/R/E} \\ dt_{IF}^{C} = dt^{C} + \frac{f_1^2}{f_1^2-f_3^2} d_1^{C} - \frac{f_3^2}{f_1^2-f_3^2} d_3^{C} \\ \quad = dt^{C} + d_1^{C} - \frac{f_3^2}{f_1^2-f_3^2} \mathrm{DCB}_{13}^{C} \end{cases} \tag{2}$$

where superscripts G, R, E and C denote the GPS, GLONASS, Galileo and BDS-3, respectively. The $\mathrm{DCB}_{12}^{G/R/E} = d_2^{G/R/E} - d_1^{G/R/E}$ and $\mathrm{DCB}_{13}^{C} = d_3^{C} - d_1^{C}$ is the frequency-dependent satellite differential code bias (DCB) that can be corrected with IGS daily solutions from BSX files (Montenbruck et al., 2014). Consequently, the satellite clock offset dt^s in Eq. (1) can be derived as

$$\begin{cases} dt^{G/R/E} = dt_{IF}^{G/R/E} - d_1^{G/R/E} + \frac{f_2^2}{f_1^2-f_2^2} \mathrm{DCB}_{12}^{G/R/E} \\ dt^{C} = dt_{IF}^{C} - d_1^{C} + \frac{f_3^2}{f_1^2-f_3^2} \mathrm{DCB}_{13}^{C} \end{cases} \tag{3}$$

By substituting Eq. (3) into Eq. (1), the new observation equation can be re-written as

$$\begin{aligned} P_{i,k}^s &= \rho_k^s + dt_{r,k} + T_k^s + \mu_i \cdot I_k^s + D_i - d_i^s + d_1^s + \varepsilon_{p_k} \\ L_{i,k}^s &= \rho_k^s + dt_{r,k} + T_k^s - \mu_i \cdot I_k^s - N_i^s + B_i - b_i^s + d_1^s + \varepsilon_{L_k} \end{aligned} \tag{4}$$

Therefore, the multi-epoch equations of S-satellites on the first frequency can be written as

$$\begin{aligned} P_k &= A_k x_k + e_s \cdot dt_{r,k} + I_k + M_k \cdot ZWD + D_1 + \varepsilon_{p_k} \\ L_k &= A_k x_k + e_s \cdot dt_{r,k} - I_k + M_k \cdot ZWD - N_1 + B_1 - b_1 + d_1 + \varepsilon_{L_k} \end{aligned} \tag{5}$$

where $P_k = \left[\mathrm{P}_k^1, \cdots, P_k^s\right]^{\mathrm{T}}$ and $L_k = \left[L_k^1, \cdots, L_k^s\right]^{\mathrm{T}}$ denote the vectors of observed-minus-computed (O-C) values for code and phase observations, respectively. A_k denotes the unit vector of the position component, and e_s is the unit vector. x_k denotes the vector of the estimated position errors. ZWD denotes the site-specific tropospheric delay error in the zenith direction, and the corresponding vectors of mapping coefficient is $M_k = \left[M_k^1, \cdots, M_k^s\right]^{\mathrm{T}}$. $I_k = \left[I_k^1, \cdots, I_k^s\right]^{\mathrm{T}}$ and $N_1 = \left[N_1^1, \cdots, N_1^s\right]^{\mathrm{T}}$ are the vectors of the ionospheric delay errors on the first frequency and integer ambiguities. $D_1 = \left[D_1^1, \cdots, D_1^s\right]^{\mathrm{T}}$ and $B_1 = \left[B_1^1, \cdots, B_1^s\right]^{\mathrm{T}}$ are the vectors of receiver hardware delays for code and phase observation, respectively. $d_1 = \left[d_1^1, \cdots, d_1^s\right]^{\mathrm{T}}$ and $b_1 = \left[b_1^1, \cdots, b_1^s\right]^{\mathrm{T}}$ are the vectors of satellite hardware delays for code and phase observation, respectively.

Since the multi-parameter correlation in Eq. (5) leads to rank deficiency of the normal equation, both satellite and receiver hardware delays can be generally incorporated into the receiver clocks and ambiguities. The newly generated receiver clock offset $\bar{dt}_{r,k}$ and ambiguity parameter $\bar{N}$ can be referenced as Eq. (6) and Eq. (7) in the literature of Wang et al., 2020. Therefore, the function model of the GNSS SF-PPP can be expressed as

$$\begin{aligned} P_k &= A_k x_k + e_s \cdot \bar{dt}_{r,k} + M_k \cdot ZWD + I_k + \delta D + \varepsilon_{p_k} \\ L_k &= A_k x_k + e_s \cdot \bar{dt}_{r,k} + M_k \cdot ZWD - I_k - \bar{N} + \varepsilon_{L_k} \end{aligned} \tag{6}$$

2.2. Ionosphere-corrected multi-GNSS single-frequency PPP model

If the line-of-sight ionospheric delay I_k in Eq. (6) is corrected by the external ionosphere model, the IC SF-PPP model with simple structure can be obtained. Although the positioning solutions of this model exist biased due to inaccurate ionospheric corrections, the IC SF-PPP model with high computational efficiency has become the most widely used SF-PPP model, especially in real-time positioning fields. In this study, four types of ionospheric models (i.e., GPS-Klobuchar, CNES-VTEC, GIM and BDGIM) are used in the IC SF-PPP model. Extending the single-system of Eq. (6) to quad-system (i.e., GPS, BDS-3, GLONASS and Galileo), the IC multi-GNSS SF-PPP model can be expressed as

$$\begin{cases} P_k^C = A_k^C x_k + e_s \cdot \bar{dt}_{r,k}^C + M_k^C \cdot ZWD + \varepsilon_{P_k}^C \\ P_k^G = A_k^G x_k + e_s \cdot \bar{dt}_{r,k}^C + ISB_k^G + M_k^G \cdot ZWD + \varepsilon_{P_k}^G \\ P_k^R = A_k^R x_k + e_s \cdot \bar{dt}_{r,k}^C + ISB_k^R + M_k^R \cdot ZWD + \delta D + \varepsilon_{P_k}^R \\ P_k^E = A_k^E x_k + e_s \cdot \bar{dt}_{r,k}^C + ISB_k^E + M_k^E \cdot ZWD + \varepsilon_{P_k}^E \\ L_k^C = A_k^C x_k + e_s \cdot \bar{dt}_{r,k}^C + M_k^C \cdot ZWD - \bar{N}_k^C + \varepsilon_{L_k}^C \\ L_k^G = A_k^G x_k + e_s \cdot \bar{dt}_{r,k}^C + ISB_k^G + M_k^G \cdot ZWD - \bar{N}_k^G + \varepsilon_{L_k}^G \\ L_k^R = A_k^R x_k + e_s \cdot \bar{dt}_{r,k}^C + ISB_k^R + M_k^R \cdot ZWD - \bar{N}_k^R + \varepsilon_{L_k}^R \\ L_k^E = A_k^E x_k + e_s \cdot \bar{dt}_{r,k}^C + ISB_k^E + M_k^E \cdot ZWD - \bar{N}_k^E + \varepsilon_{L_k}^E \end{cases} \tag{7}$$

where the receiver clock offset $\bar{dt}_{r,k}^C$ is set to BDS-3 system. For other GNSSs, the inter-system bias (ISB)

$ISB = \left[ISB^1, \cdots, ISB^s\right]^{\mathrm{T}}$ is required to compensate for the time offsets of different systems. The vector of estimable parameters X for IC model can be expressed as

$$X = \left[x, \bar{dt}_r^C, ISB^{G/R/E}, ZWD, \delta D, \bar{N}^{C/G/R/E}\right] \tag{8}$$

2.3. Ionosphere-free multi-GNSS single-frequency PPP model

Due to the fact that the ionospheric errors of one satellite are the same for both code and phase observations, but the symbols are opposite, the ionospheric errors in SF-PPP can be eliminated by forming the GRAPHIC combination (Montenbruck, 2003). This model has the ability to obtain much better positioning accuracy compared with the IC model, but its initialization time may be adversely affected due to the large noise of the GRAPHIC observations (Wang et al., 2020b; Chen et al., 2022). As to multi-GNSS with quad-constellation, the IF SF-PPP model can be expressed as

$$\begin{cases} \frac{P_k^C+L_k^C}{2} = A_k^C x_k + e_s \cdot \bar{dt}_{r,k}^C + M_k^C \cdot ZWD - \frac{\bar{N}_k^C}{2} + \frac{\varepsilon_{P_k}^C+\varepsilon_{L_k}^C}{2} \\ \frac{P_k^G+L_k^G}{2} = A_k^G x_k + e_s \cdot \bar{dt}_{r,k}^C + ISB_k^G + M_k^G \cdot ZWD - \frac{\bar{N}_k^G}{2} + \frac{\varepsilon_{P_k}^G+\varepsilon_{L_k}^G}{2} \\ \frac{P_k^R+L_k^R}{2} = A_k^R x_k + e_s \cdot \bar{dt}_{r,k}^C + ISB_k^R + M_k^R \cdot ZWD + \frac{\delta D}{2} - \frac{\bar{N}_k^R}{2} + \frac{\varepsilon_{P_k}^R+\varepsilon_{L_k}^R}{2} \\ \frac{P_k^E+L_k^E}{2} = A_k^E x_k + e_s \cdot \bar{dt}_{r,k}^C + ISB_k^E + M_k^E \cdot ZWD - \frac{\bar{N}_k^E}{2} + \frac{\varepsilon_{P_k}^E+\varepsilon_{L_k}^E}{2} \end{cases} \tag{9}$$

where the number of observation equations in the IF model is only half of that of the IC model, thus the code equations in Eq. (7) need to be introduced into the IF model to solve the problem of rank deficiency in the normal equation. Note that the ionospheric errors in code observations can be ignored because the weight of the code observations in the IF SF-PPP model is very low, and this slight impact is only shown in the early convergence stage. The vector of estimable parameters X for IF model can be expressed as

$$X = \left[x, \bar{dt}_r^C, ISB^{G/R/E}, ZWD, \frac{\delta D}{2}, \frac{\bar{N}^{C/G/R/E}}{2}\right] \tag{10}$$

2.4. Ionosphere-weighted multi-GNSS single-frequency PPP model

In addition to forming the GRAPHIC observations, the ionospheric errors can also be completely eliminated by estimating the ionospheric parameter in the undifferenced and uncombined PPP model (Liu et al., 2017). To avoid the rank deficiency of the normal equations due to the increase of estimated ionospheric parameters, the virtual observation equations based on the external ionospheric corrections need to be added as the constraints in the SF-PPP model. Therefore, the IW model in multi-GNSS SF-PPP can be expressed as

$$\begin{cases} P_k^C = A_k^C x_k + e_s \cdot \bar{dt}_{r,k}^C + M_k^C \cdot ZWD + I_k^C + \varepsilon_{P_k}^C \\ P_k^G = A_k^G x_k + e_s \cdot \bar{dt}_{r,k}^C + ISB_k^G + M_k^G \cdot ZWD + I_k^G + \varepsilon_{P_k}^G \\ P_k^R = A_k^R x_k + e_s \cdot \bar{dt}_{r,k}^C + ISB_k^R + M_k^R \cdot ZWD + I_k^R + \varepsilon_{P_k}^R \\ P_k^E = A_k^E x_k + e_s \cdot \bar{dt}_{r,k}^C + ISB_k^E + M_k^E \cdot ZWD + I_k^E + \varepsilon_{P_k}^E \\ L_k^C = A_k^C x_k + e_s \cdot \bar{dt}_{r,k}^C + M_k^C \cdot ZWD - I_k^C - \bar{N}_k^C + \varepsilon_{L_k}^C \\ L_k^G = A_k^G x_k + e_s \cdot \bar{dt}_{r,k}^C + ISB_k^G + M_k^G \cdot ZWD - I_k^G - \bar{N}_k^G + \varepsilon_{L_k}^G \\ L_k^R = A_k^R x_k + e_s \cdot \bar{dt}_{r,k}^C + ISB_k^R + M_k^R \cdot ZWD - I_k^R - \bar{N}_k^R + \varepsilon_{L_k}^R \\ L_k^E = A_k^E x_k + e_s \cdot \bar{dt}_{r,k}^C + ISB_k^E + M_k^E \cdot ZWD - I_k^E - \bar{N}_k^E + \varepsilon_{L_k}^E \\ \tau_k^{C/G/R/E} = I_k^{C/G/R/E} + \varepsilon_{\tau_k}^{C/G/R/E} \end{cases} \tag{11}$$

where τ_k denotes the ionospheric delays obtained from the high-precision external ionospheric models, such as the GIM, CNES-VTEC and BDGIM. $\varepsilon_{\tau_k}^{C/G/R/E}$ is the noise of virtual ionospheric observables.

To obtain the ideal convergence performance of the IW SF-PPP, the weight of virtual ionospheric observations needs to be set as accurately as possible (Li et al., 2019). In order to ensure that all selected stations distributed globally have similar ionospheric constraint accuracy, this study adopts the spatial–temporal correlation-constrained method that considers both latitude and local time simultaneously (Zhang et al., 2013). The prior variance of the ionospheric parameter σ_{ion}^2 can be expressed as

$$\sigma_{ion}^2 = \frac{1}{m^2} \cdot \begin{cases} \sigma_{ion,0}^2 + \sigma_{ion,1}^2 \cdot \cos(B_{IPP}) \cdot \cos\left(\frac{t_{IPP}-14}{12}\pi\right), & 8 < t_{IPP} < 20 \text{ or } B_{IPP} < \frac{\pi}{3} \\ \sigma_{ion,0}^2, & otherwise \end{cases} \tag{12}$$

$$m = \sqrt{1 - \frac{\sin^2 Z}{(1 + H_{ion}/R_{Earth})}} \tag{13}$$

where m denotes the mapping function of ionospheric delay conversion. Z denotes the zenith angle of the receiver. H_{ion} denotes the height of the single layer, which is 400 km, 450 km and 450 km for the BDGIM, CNES-VTEC and GIM models, respectively. R_{earth} is the average radius of the Earth in kilometer. B_{IPP} is the latitude of the ionospheric pierce point (IPP), and t_{IPP} is the local time in hours. $\sigma_{ion,0}^2$ denotes the variance of the ionospheric delay in the zenith direction, and $\sigma_{ion,1}^2$ denotes the variation of the ionospheric delay. Both $\sigma_{ion,0}^2$ and $\sigma_{ion,1}^2$ are empirical parameters obtained from the precision of the external ionospheric model. Given that the ionospheric correction accuracy of the BDGIM, CNES-VTEC and GIM models decreases in turn (Wang et al., 2019; 2020a; Zhang et al., 2022), the corresponding both $\sigma_{ion,0}$ and $\sigma_{ion,1}$ are generally set as 0.5, 0.4 and 0.3 m, respectively. As for the GPS Klobuchar model, the ionospheric prior variance can be set as the square of the calculated ionospheric corrections (Wang et al., 2019).

As to the IW model, the vector of estimable parameters X for multi-GNSS SF-PPP can be expressed as

$$X = \left[x, d\bar{t}_r^C, ISB^{G/R/E}, ZWD, I^{C/G/R/E}, \bar{N}^{C/G/R/E}\right] \quad (14)$$

In addition, we also need to propose the stochastic model of the multi-GNSS SF-PPP. There are two modeling options for different estimable parameters, i.e., white noise process and random walk process. The station coordinates and receiver clock are estimated as white noise processing, which can be referred to Eq. (4) in the literature of Zhou et al., 2020. The ionospheric delay, tropospheric delay and ISB parameters are considered as the random walk process, and the specific formula can be referred to Eq. (14) in the literature of Zhou et al., 2019.

3. Experiment data and processing strategy

In order to investigate the contribution of BDS-3 to multi-GNSS SF-PPP performance on a global scale, the positioning tests were conducted using data from multi-GNSS experiment (MGEX) stations uniformly distributed worldwide. In addition, the specific processing strategies of the BDS-3/GNSS combined SF-PPP are summarized in this section.

3.1. Datasets

The BDS-3/GPS/GLONASS/Galileo observations with the interval of 30 s were collected from 27 global MGEX stations, and the distribution of these selected stations can be shown in Fig. 1. The test period is set to DoY (Day of Year) 218–224 in 2022. For the ionospheric changes and solar activity, the geomagnetic Kp and radio flux index F10.7 values during the whole experiment are presented in Fig. 2. We can see that the F10.7 index was relatively high and changed between 110.5 and 122.7 sfu during the testing period. The ionospheric conditions were quiet or unsettled as the Kp index is between 0.33 and 2.67 in DoY 218 and 224, while for other days, the ionospheric conditions were relatively active since most Kp indexes exceed 3 or even reach 5.67.

3.2. Processing strategies

The Net_Diff software (https://center.shao.ac.cn/shao_gnss_ac/Net_diff/Net_diff. html) was used to carry out multi-GNSS SF-PPP with different ionospheric models in simulated kinematic mode. The GBM orbits and clocks provided by GFZ are utilized to correct orbit and clock errors in this study. The tidal effects, including solid tides, polar tides, and ocean-loading tides, have been corrected using corresponding models. Some minor corrections also need to be considered, such as relativistic, phase windup and earth rotation. Note that the known coordinates of all selected MGEX stations within 1.0 cm accuracy are obtained from the IGS SINEX (Solution-INdependent EXchange) file. Besides, the main processing strategies and adopted error correction models of BDS-3/GNSS SF-PPP are shown in Table 1.

4. Results and discussion

In this section, the positioning results of the BDS-3/GNSS SF-PPP with different ionospheric models are given from the IC, IF, and IW strategies, respectively. Before discussing the contribution of BDS-3 to the multi-GNSS SF-PPP, the number of available satellites and PDOP

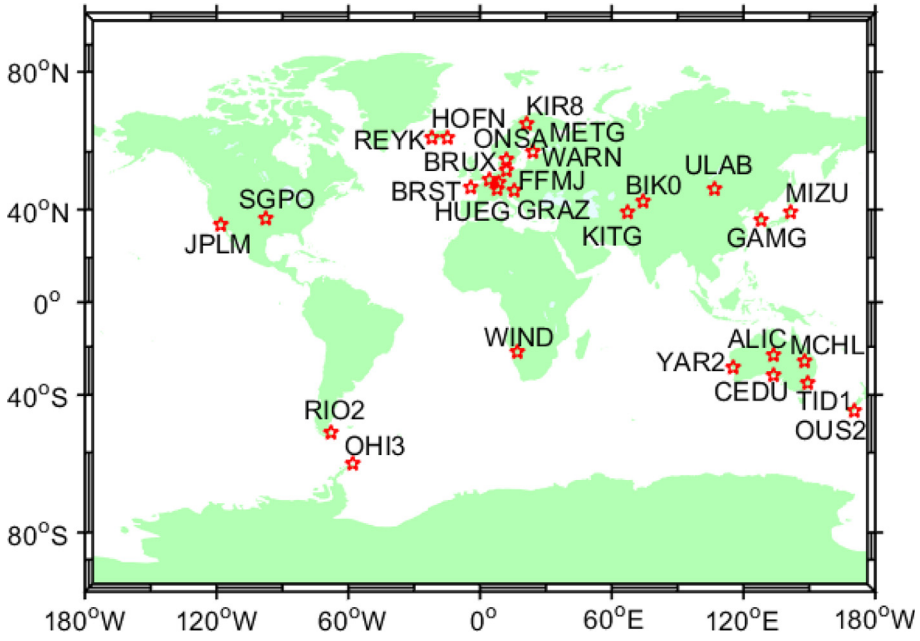

Fig. 1. Distribution of all selected MGEX stations.

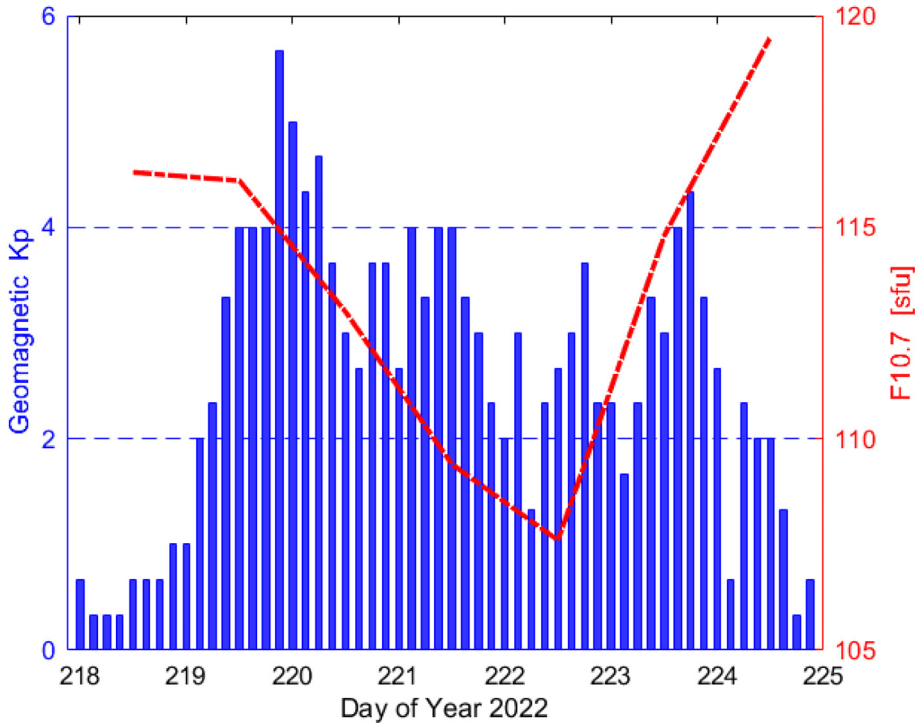

Fig. 2. Geomagnetic Kp and radio flux index F10.7 values in the test period.

Table 1
Processing strategies and error correction models used in the experiment.

Item	Strategies/models
Observations	Code + Carrier phase
Frequency	BDS-3: B1; GPS/GLONASS: L1; Galileo: E1
Elevation cutoff angle	7°
Priori variance of observations	0.3/0.3/0.6/0.3 and 0.003/0.003/0.003/0.003 m for the BDS-3/GPS/GLONASS/Galileo raw code and phase, respectively
Weighing strategies	Elevation-dependent weighing model (Zhang et al., 2020);
PCO (Phase Center Offset) and PCV (Phase Center Variation) (PCV)	Corrected with igs14_2188.atx file
Satellite DCB	Corrected with IGS daily solutions from DLR.BSX files
Estimator	Kalman filter
Tropospheric delay	Dry part is corrected by GPT2w + SAAS + VMF (Boehm et al., 2015); wet part is estimated as random-walk noise (Zhou et al., 2019)
Ionospheric delay and ISB	Random-walk noise estimation (Zhou et al., 2019)
Station coordinates and receiver clock	White noise estimation (Zhou et al., 2019)
GLONASS IFCB	Estimated as a linear function of signal frequency (Zhou et al., 2018)
Phase ambiguities	Float solution

(Position Dilution Of Precision) values for all selected stations need to be evaluated first, because the constellation geometry has a direct impact on PPP performance.

4.1. Number of available satellites and PDOP values

Fig. 3 shows the mean number of available satellites at the 27 MGEX stations when the elevation angle exceeds 10 degrees for different systems during the test period. It is obvious that the available satellites of GPS are more than that of other systems for all selected stations, with an average number of 9.2 to 10.7. GLONASS has the least number of available satellites with 5.5 to 6.9. The average number of BDS-3 satellites is comparable with Galileo, which varies from 7.0 to 9.1 for all stations. Correspondingly, the mean PDOP of all used stations in the same period is given in Fig. 4. Compared with the GLONASS PDOP between 2.4 and 3.2, the average PDOP of GPS, BDS-3 and Galileo are clearly lower with 1.6–1.8, 1.9–2.3 and 1.8–2.4, respectively. Therefore, the geometry of GPS has the best performance in this experiment, and the sufficient observations of BDS-3/Galileo have the ability to support high-precision

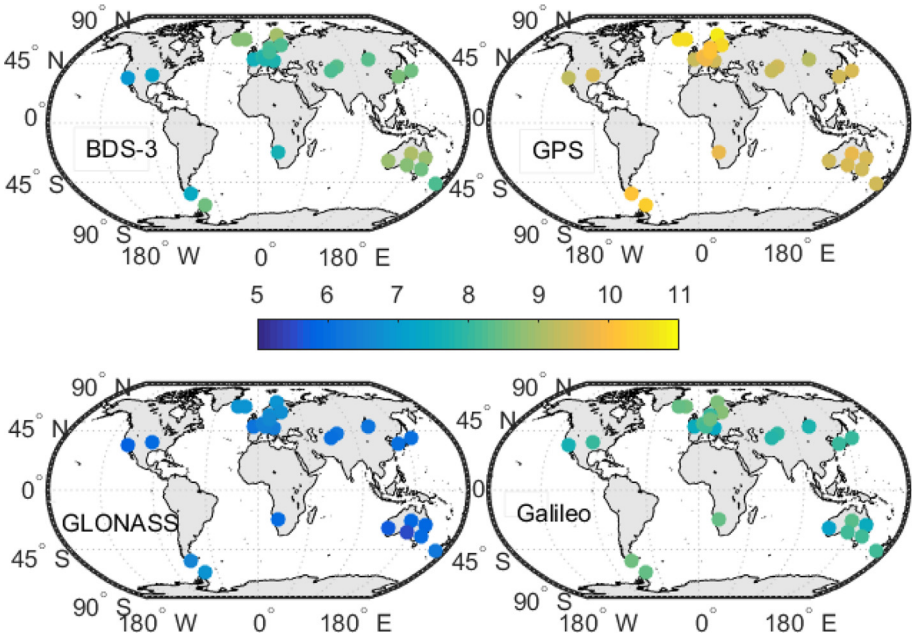

Fig. 3. Mean number of available satellites for different GNSSs at 27 MGEX stations (DoY 218–224, 2022).

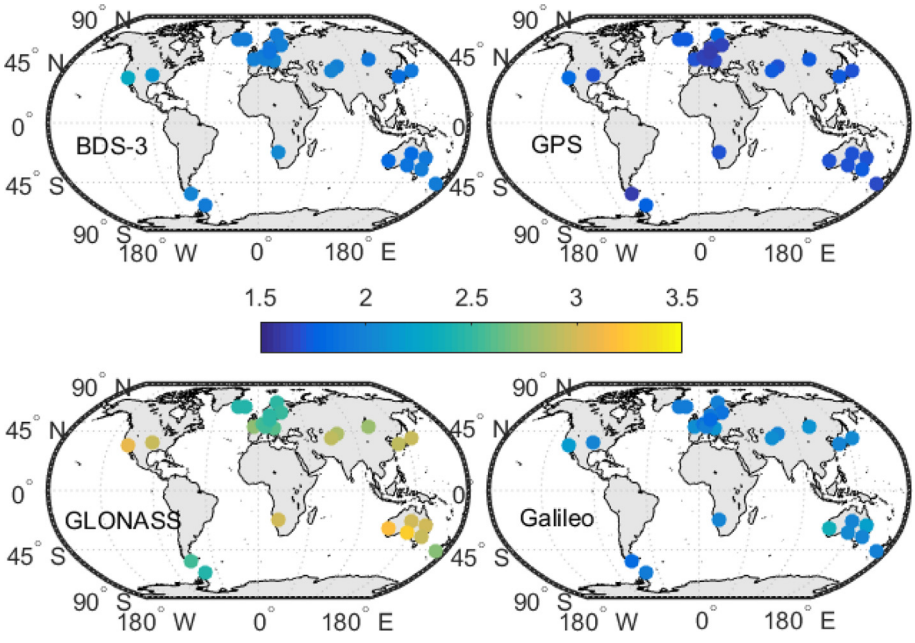

Fig. 4. Mean PDOP of different GNSSs at 27 MGEX stations (DoY 218–224, 2022).

positioning solutions. While for GLONASS, due to the limited available satellites, it is difficult to achieve ideal positioning performance in theory.

4.2. Ionosphere-corrected BDS-3/GNSS single-frequency PPP

Among all the ionospheric models used in this study, the GPS Klobuchar has the worst performance, with an ionospheric correction rate of only about 55 % globally (Orus et al., 2002). As for the BDGIM model, its ionospheric correction capability can be up to 77.6 and 80.9 % on a global scale and in the Chinese region, respectively (Yuan et al., 2019). At present, the GIM model has the highest ionospheric correction accuracy, with about 2 to 4 TECU (total electron content unit) in most parts of the world. After long-term quality assessment, the performance of CNES-VTEC products is comparable to the GIM model (Nie et al., 2019; Wang et al., 2020a).

Since the ionospheric condition of DoY 220 is the most active during the test period, the positioning errors of IC SF-PPP in kinematic mode at FFMJ station on this day

are selected as the example of daily solutions (seen in Fig. 5). Note that C, G, R and E denote the BDS-3, GPS, GLONASS and Galileo systems, respectively. Whether for single- or multi-GNSS, the positioning results of IC SF-PPP based on the GIM model have the best performance, which is reasonable given that the ionospheric correction accuracy of the GIM model can be up to 2 TECU. As to the three real-time ionospheric models, the positioning accuracy of CNES-VTEC products is better than that of both BDGIM and GPS Klobuchar, meanwhile, the performance of BDGIM in the IC SF-PPP domain is significant superiority to GPS Klobuchar. No matter what kind of ionospheric model is used in IC SF-PPP, with the introduction of BDS-3 observations, the positioning errors of GPS + BDS-3, GLONASS + BDS-3 and Galileo + BDS-3 in the N (North), E(East) and U (Up) components can be reduced in different levels. Especially for GLONASS with limited available satellites, the GLONASS + BDS-3 positioning performance is evidently superior to the GLONASS-only solutions. When integrating quad-system observations, the positioning errors of IC SF-PPP using CNES-VTEC or BDGIM models in all directions can be kept within 1.0 m. If the above ionospheric model is replaced by GIM, the corresponding positioning errors can even be stabilized within 0.5 m.

Fig. 6 shows the RMS of positioning errors of IC SF-PPP in kinematic mode for all stations during the testing period. The improvement rates of positioning accuracy for multi-GNSS solutions in comparison with the single-GNSS solutions is summarized in Table 2. It can be seen that the positioning accuracy of GLONASS-only IC SF-PPP is the worst among all single- or multi-GNSS solutions, which RMS values of 0.58–0.97 m in horizontal and 1.06–1.62 m in vertical for different ionospheric models. By introducing the BDS-3 observations, its 3D positioning accuracy can be significantly improved by at least 32.1 %. The main reason is that the number of visible satellites in the GLONASS + BDS-3 solution can be increased by more than twice compared to the GLONASS-only solution, as shown in Fig. 3. For each ionospheric model, the positioning accuracy of both GPS-only and Galileo-only IC SF-PPP has similar performance, its RMS errors are 0.21–0.60 m and 0.41–0.93 m in the horizontal and vertical components, respectively. Correspondingly, with the introduction of BDS-3 observation, the 3D positioning accuracy can be improved by 7.4–11.6 % and 6.9–12.9 % for GPS-only and Galileo-only solutions, respectively. Note that the improvements of 7.4 % with GPS + BDS-3 and 6.9 % with Galileo + BDS-3 are all for BDGIM model. In regard to the BDS-only IC SF-PPP solutions, the posi-

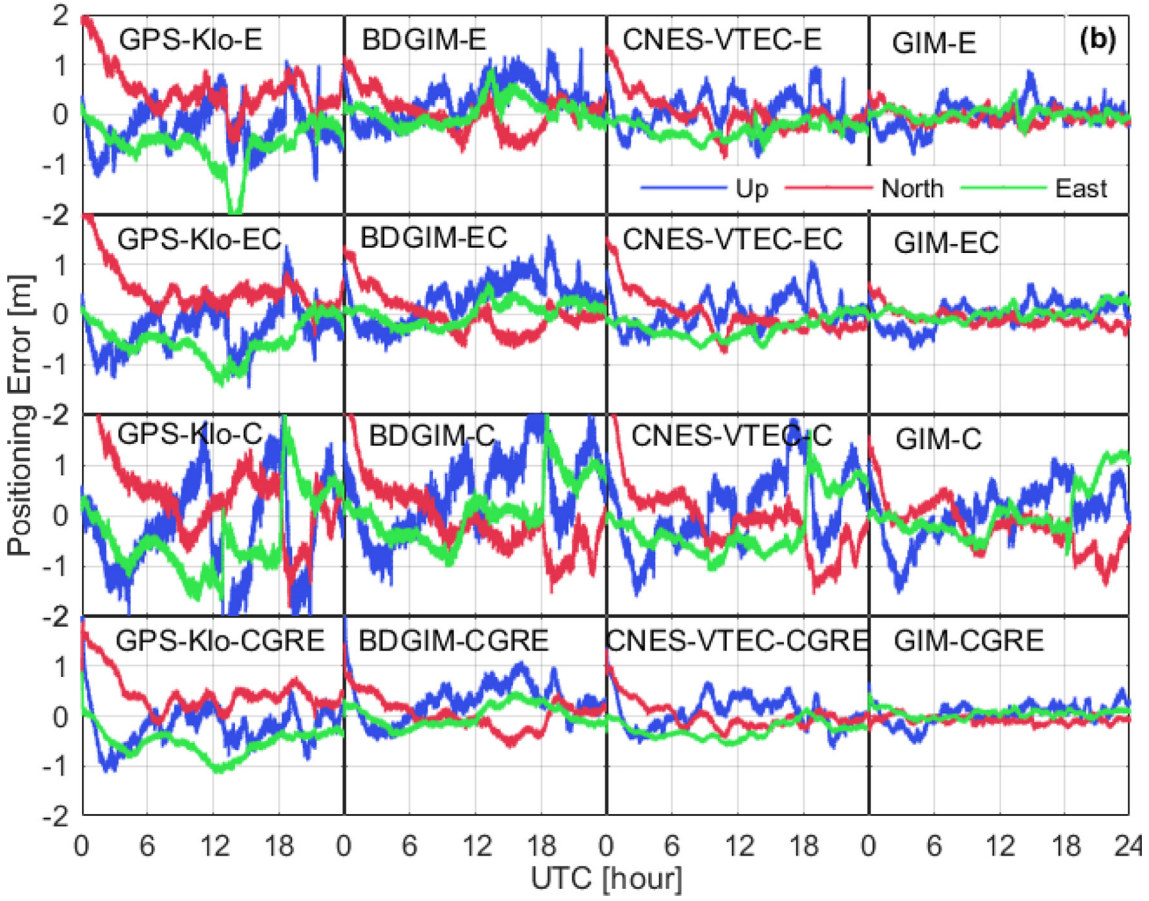

Fig 5. *(continued)*

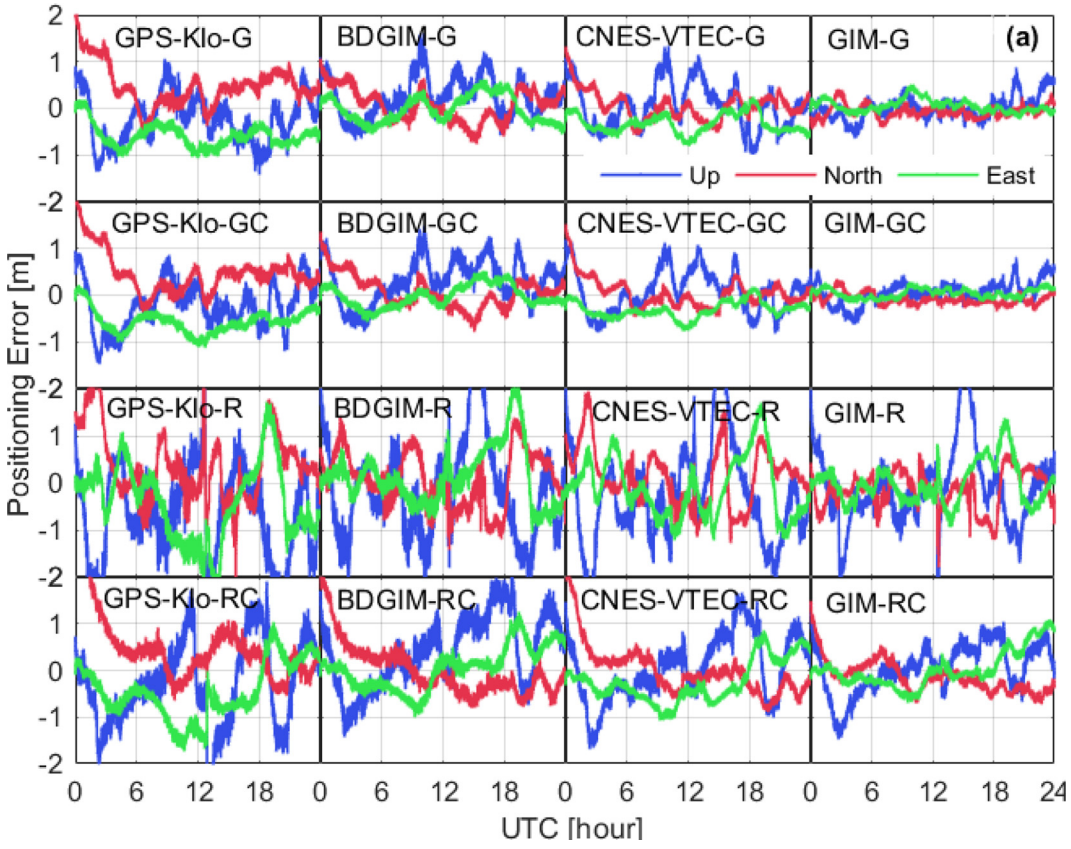

Fig. 5. Positioning errors of IC SF-PPP with different scenarios at FFMJ station in kinematic mode (DoY 220, 2022).

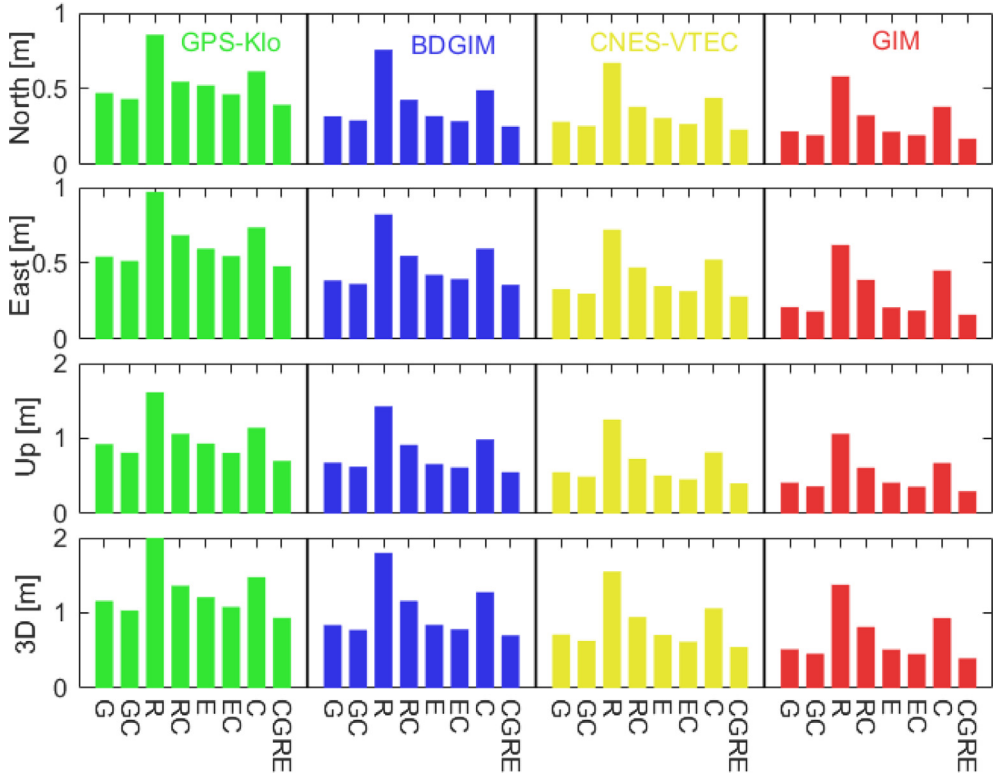

Fig. 6. RMS of positioning errors of IC SF-PPP in kinematic mode (27 MGEX stations, DoY 218–224, 2022).

Table 2
Improvement rates of the positioning accuracy of IC SF-PPP for the GNSS + BDS-3 solutions compared to single-GNSS solutions (unit: %).

Ionospheric model	Component	G vs GC	R vs RC	E vs EC	C vs CGRE
GPS Klobuchar	North	8.4	36.2	11.3	35.9
	East	5.3	29.5	8.1	34.7
	Up	12.3	34.3	13.2	38.5
	3D	10.9	32.1	10.5	36.7
BDGIM	North	8.8	43.5	10.3	48.7
	East	5.9	33.3	6.8	39.8
	Up	8.2	36.0	7.0	44.2
	3D	7.4	35.5	6.9	45.0
CNES-VTEC	North	10.2	43.2	12.7	47.2
	East	9.4	34.6	9.4	46.3
	Up	10.5	41.9	10.4	50.3
	3D	11.6	39.0	12.9	48.7
GIM	North	11.4	44.1	10.1	55.4
	East	12.8	37.0	9.6	64.5
	Up	12.1	42.4	13.6	55.7
	3D	11.2	41.0	11.9	57.4

tioning accuracy can reach 0.38–0.74 m and 0.68–1.14 m in the horizontal and vertical components, respectively, when using different ionospheric models. Its performance is clearly worse than that of both GPS-only and Galileo-only solutions. One reason is that the constellation geometry of BDS-3 during the experiment is not as good as GPS and Galileo, as shown in Figs. 3 and 4. Another reason is that the quality of BDS-3 precise products like orbits and clocks is currently inferior to both GPS and Galileo. In all multi-GNSS solutions, the BDS-3 + GPS + GLO NASS + Galileo IC SF-PPP has the best performance, with the 3D RMS of 0.94, 0.70, 0.55 and 0.40 m for the GPS Klobuchar, BDGIM, CNES-VTEC and GIM models, respectively.

4.3. Ionosphere-free BDS-3/GNSS single-frequency PPP

The residual ionospheric errors after external ionospheric correction give rise to biased positioning results in the IC SF-PPP solution (seen in Fig. 5), so their positioning errors may vary between a few meters. However, the positioning errors of the IF SF-PPP solution have the ability to maintain below 0.3 m after convergence of several minutes. Therefore, the convergence of the IF SF-PPP can be evaluated, which is a key indicator of concern for SF-PPP users. Fig. 7 depicts the convergence curve of kinematic IF SF-PPP at the 68 % confidence level in the first 2.5 h. In this statistics, the absolute positioning errors of 27 stations in 7 days at each epoch ($27 \times 7 = 189$ values) were sorted from small to large, and then we collected the values below 68 % of all absolute positioning errors at each epoch (Lou et al., 2016). It should be noted that the GLONASS-only results of IF SF-PPP cannot be evaluated in this study, because its average number of available satellites for more than half of the selected 27 stations is only 5–6 (seen in Fig. 3), which always leads to re-converge frequently in daily solution and cannot obtain the stable and continuous positioning curve. From Fig. 7, we can see that the convergence time of GPS/Galileo/BDS-3-only IF SF-PPP with the horizontal positioning errors being 0.3 m is about 62.0/116.5/108.5 min. While for the vertical component, the positioning error of both Galileo-only and BDS-only solutions cannot converge to 0.3 m. The GPS-only IF SF-PPP still has the best vertical convergence performance with 75.5 min in all the single-GNSS solutions. By adopting the BDS-3/GNSS combined strategies, the convergence time of the GPS/Galileo-only can be shortened by 39.5/65.7 % to 37.5/40.0 min in the horizontal component. In terms of the vertical convergence, the improvements of GPS + BDS-3 and Galileo + BDS-3 solutions are about 23.7 and 57.5 % and can up to 58.0 and 66.5 min, respectively. Compared with the BDS-only IF SF-PPP, the horizontal convergence time of the GLONASS + BDS-3 can be greatly reduced from 108.5 to 71.5 min, and its positioning errors in vertical can be lower than 0.3 m within 89.0 min. When the quad-system observations are processed together, the number of available satellites can be up to 35–40, as shown in Fig. 3. Therefore, its convergence performance is the best as expected, with approximately 14.5 and 23.5 min in the horizontal and vertical components, respectively.

Fig. 8 summarizes the RMS of positioning errors of IF SF-PPP in kinematic mode for all selected stations during the testing period, and the improvement rates of positioning accuracy for multi-GNSS solutions compared to single-GNSS solutions is given in Table 3. Note that the positioning errors after 2 h of convergence in daily solutions are collected for computation. As we can see, the positioning accuracy of horizontal within 0.25 m is better than that of vertical within 0.3 m in all IF SF-PPP solutions. For single-GNSS solutions, GPS-only has the best positioning accuracy with 0.110, 0.132, and 0.220 m in the N, E, and U components, respectively, due to the optimal PDOP value (seen in Fig. 4). The positioning accuracy

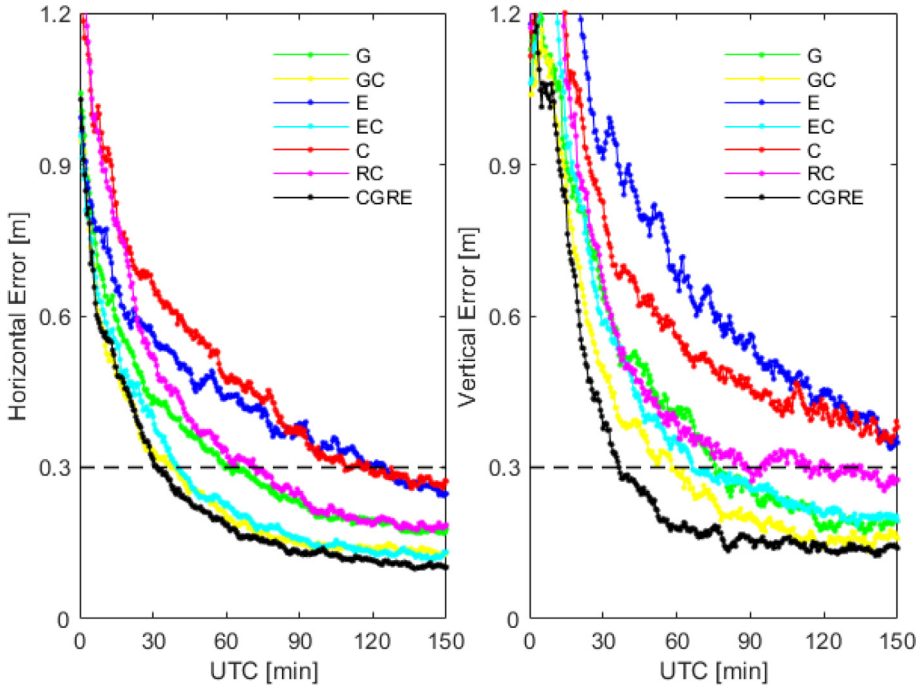

Fig. 7. Convergence performance of kinematic IF SF-PPP with different solutions at the 68% confidence level (27 MGEX stations, DoY 218–224, 2022).

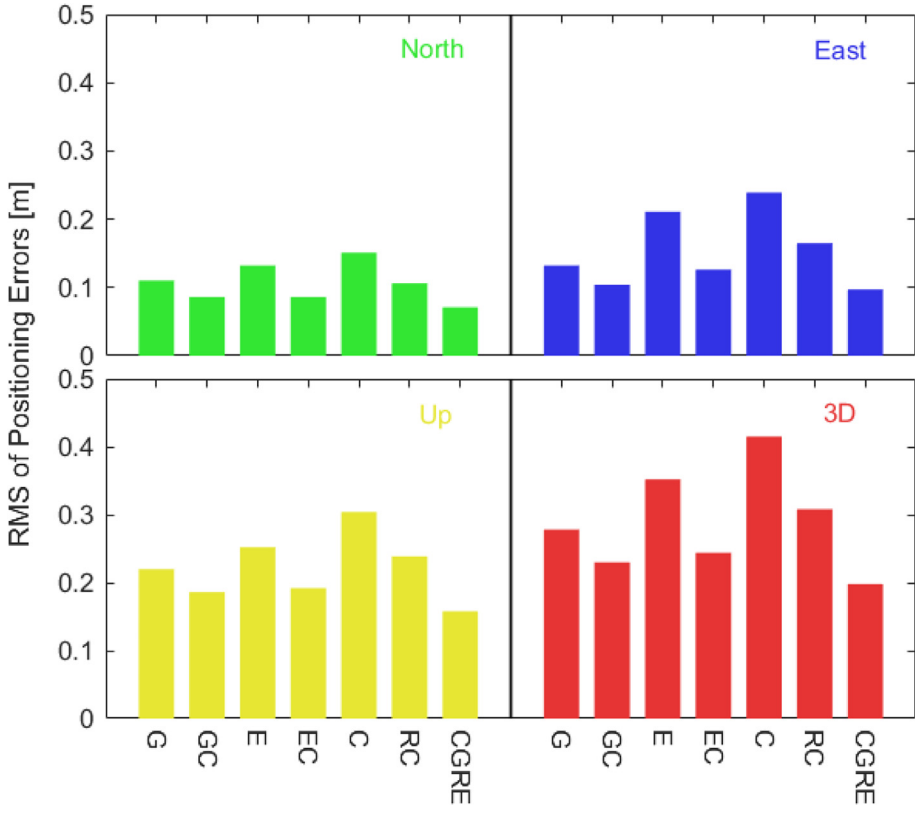

Fig. 8. RMS of positioning errors of IF SF-PPP in kinematic mode (27 MGEX stations, DoY 218–224, 2022).

of the Galileo-only solution, with RMS values of 0.211 m in horizontal and 0.252 m in vertical, is slightly better than that of the BDS-3-only solution. As to multi-GNSS solutions, the 3D positioning accuracy of GPS + BDS-3 and Galileo + BDS-3 solutions can be improved by 17.3 % to 0.230 m and 30.7 % to 0.244 m, respectively, compared with the GPS-only and Galileo-only IF SF-PPP. With the support of GLONASS observations, the 3D positioning

Table 3
Improvement rates of the positioning accuracy of IF SF-PPP for the GNSS + BDS-3 solutions compared to single-GNSS solutions (unit: %).

Component	G vs GC	E vs EC	C vs RC	C vs CGRE
North	21.8	34.9	29.8	53.0
East	21.2	40.3	31.0	59.4
Up	15.5	23.8	21.4	48.0
3D	17.3	30.7	25.8	52.3

accuracy can be clearly improved from 0.415 m of the BDS-3-only solution to 0.308 m of the GLONASS + BDS-3 solution, with an improvement rate of up to 25.8 %. Similar to the convergence performance, the positioning accuracy of the BDS-3 + GPS + Galileo + GLONASS IF SF-PPP has the ability to be optimal and its 3D RMS can be less than 0.2 m, which is 2–5 times better than that of quad-system IC SF-PPP using different ionospheric models (as shown in Fig. 6).

4.4. Ionosphere-weighted BDS-3/GNSS single-frequency PPP

The IF SF-PPP has the ability to achieve 0.2–0.3 m high-precision positioning, but its convergence performance is not satisfactory due to the increase of observation noise. In order to improve the convergence performance of SF-PPP on the basis of ensuring high positioning accuracy, the IW SF-PPP model has been applied widely. Fig. 9 shows the convergence curve of kinematic IW SF-PPP based on the different ionospheric models at the 68 % confidence level in the first 2.5 h. Here, the results of kinematic IF SF-PPP are set as the reference values. As shown in Fig. 9 (a), the convergence performance of both CNES-VTEC- and GIM-constrained SF-PPP in all components for GPS-only or GPS + BDS-3 solutions during the first 60 min is much better than that of the corresponding IF SF-PPP solutions. While for BDGIM-constrained SF-PPP, its convergence performance of only first 15 min in horizontal and 30 min in vertical for both GPS-only and GPS + BDS-3 is better than that of IF SF-PPP solutions. Due to the insufficient accuracy of the ionospheric correction capability for the GPS Klobuchar model, the positioning errors of the first 30 min in both horizontal and vertical components for the GPS Klobuchar-constrained SF-PPP solution are even worse than that for IF SF-PPP solution. Compared with the positioning errors of IF SF-PPP at the first epoch with 0.95 m in horizontal and 1.10 m in vertical, the results of GPS Klobuchar-, BDGIM-, CNES-VTEC- and GIM-constrained SF-PPP can reach 1.31, 0.60, 0.58 and 0.43 m in horizontal and 1.73, 1.05, 0.91 and 0.65 m in vertical, respectively.

From Fig. 9(b), compared with the Galileo-only IF SF-PPP, the convergence performance of all ionospheric-constrained Galileo-only SF-PPP solutions in both horizontal and vertical components can be significantly improved during the first 150 min. Interestingly, with the introduction of BDS-3 observations, the apparent improvements of horizontal convergence in Galileo + BDS-3 IW SF-PPP are only presented in the first 15, 35 and 45 min of BDGIM, CNES-VTEC and GIM models, respectively. More importantly, within the first 30 min, the corresponding convergence performance of the GPS Klobuchar-constrained solution is even worse than that of the IF solution. However, for the vertical convergence performance, the Galileo + BDS-3 IW SF-PPP based on the different ionospheric models has always maintained the advantage over the Galileo + BDS-3 IF SF-PPP.

As to Fig. 9(c), the BDS-3-only and BDS-3 + GLONASS IF SF-PPP show basically the same convergence performance during the first 30 min, while in the period of 30 to 150 min, the results of BDS-3 + GLONASS have a distinct superiority compared with the BDS-3-only solution. Different from the IF SF-PPP solution, the convergence performance of BDS-3 + GLONASS IW SF-PPP is better than that of BDS-3-only results for all kinds of ionospheric models during the first 150 min. This phenomenon presents the advantages of the IW SF-PPP model in the case of integrating GLONASS observations in the initialization period. In the BDS-3 + GPS + GLONASS + Galileo solution, the convergence performance of GPS Klobuchar-, BDGIM-, CNES-VTEC- and GIM-constrained IW SF-PPP increases successively. Except for the GPS Klobuchar-constrained solution, the convergence performance of the IW SF-PPP is better than that of the IF SF-PPP, and its positioning errors at the first epoch have the ability to reach within 0.5 m in both horizontal and vertical components.

Fig. 10 summarizes the average convergence time of IF/IW solutions in kinematic mode at the 68 % confidence level for all selected stations during the whole experiment. Note that the convergence criterion is defined as the positioning error below 0.3 m (Wang et al., 2019). The improvement rates of the converge time for different IW solutions compared to the IF solution are shown in Table 4. As we can see, in all single- or multi-GNSS IW SF-PPP except for the GLONASS + BDS-3 solution, the GIM-constrained SF-PPP has the shortest convergence time in the horizontal and vertical components, which is reasonable given that the GIM model as a post-processed ionospheric product has the best performance at present. With the introduction of the BDS-3 observations for GIM-constrained SF-PPP, the vertical convergence time of the GPS/Galileo-only solutions can be significantly reduced, but this reduction cannot be presented in the horizontal component. When the GLONASS observations are applied into the BDS-3-only GIM-constrained SF-PPP, the convergence time can be reduced in both horizontal and vertical components, with the improvements of 15.3 and 23.2 %, respectively. The above convergence improvement of the BDS-3 + GNSS solutions is attributed to the reduction of PDOP and the optimization of constellation geometry. In case of the quad-system observations processing simultaneously, the convergence time of the GIM-

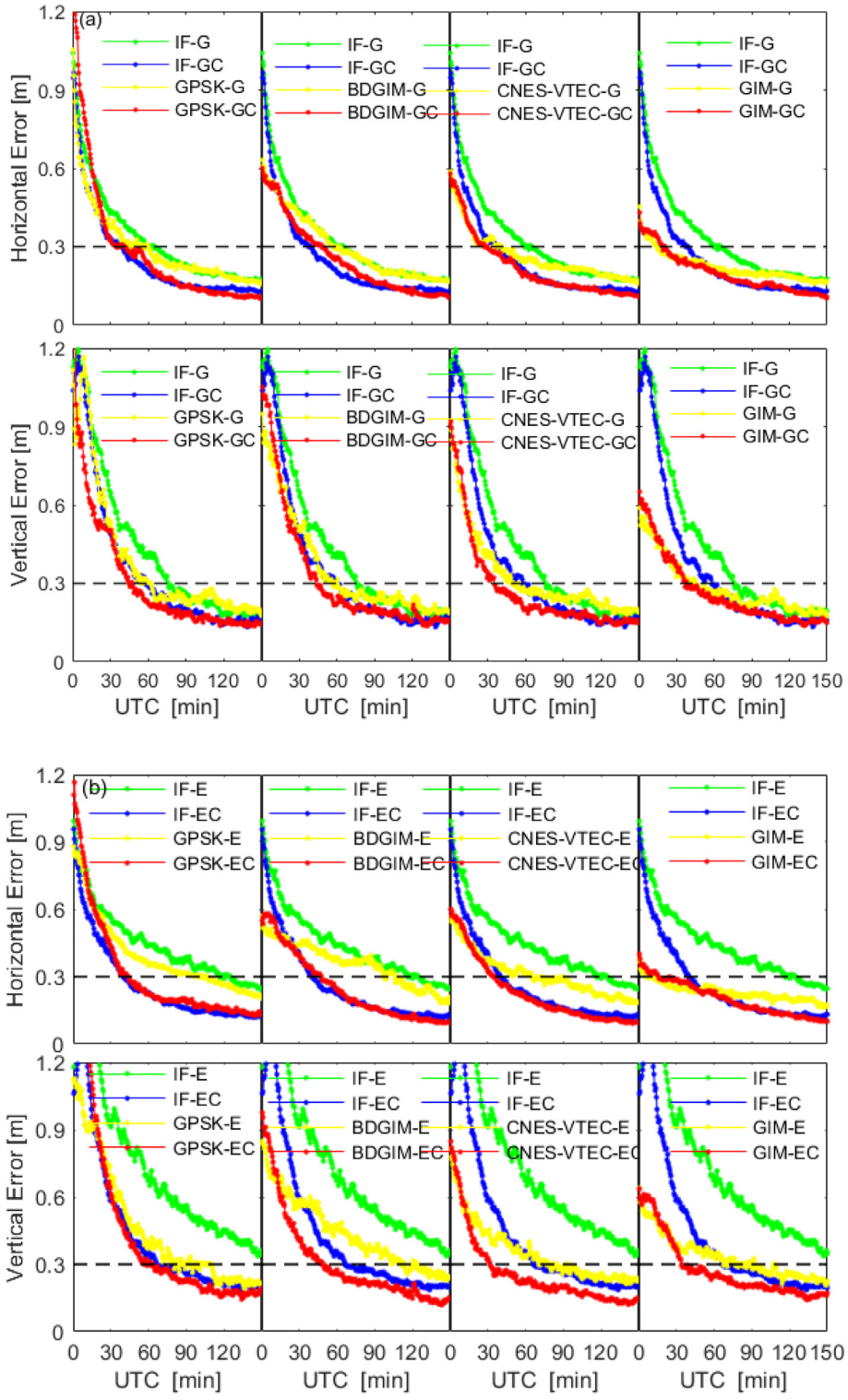

Fig. 9. Convergence performance of kinematic IF/IW SF-PPP at the 68% confidence level for (a) BDS-3/GPS, (b) BDS-3/Galileo and (c) BDS-3/GPS/GLONASS/Galileo solutions (27 MGEX stations, DoY 218–224, 2022).

constrained SF-PPP can be reduced to 5.5 and 26.0 min in the horizontal and vertical components, respectively, which is improved by 82.8 % in horizontal and 29.7 % in vertical compared to the IF SF-PPP solution. This shows that the GIM-constrained SF-PPP has the ability to achieve fast horizontal convergence.

For the real-time ionospheric models, the convergence time of the CNES-VTEC-constrained SF-PPP is much

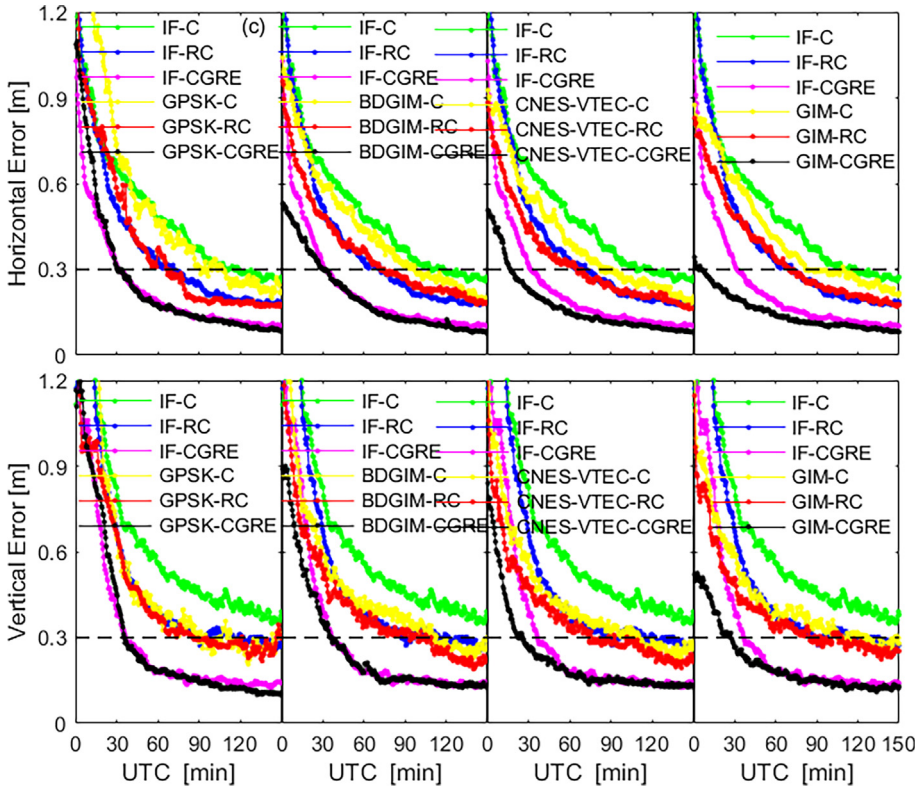

Fig 9. *(continued)*

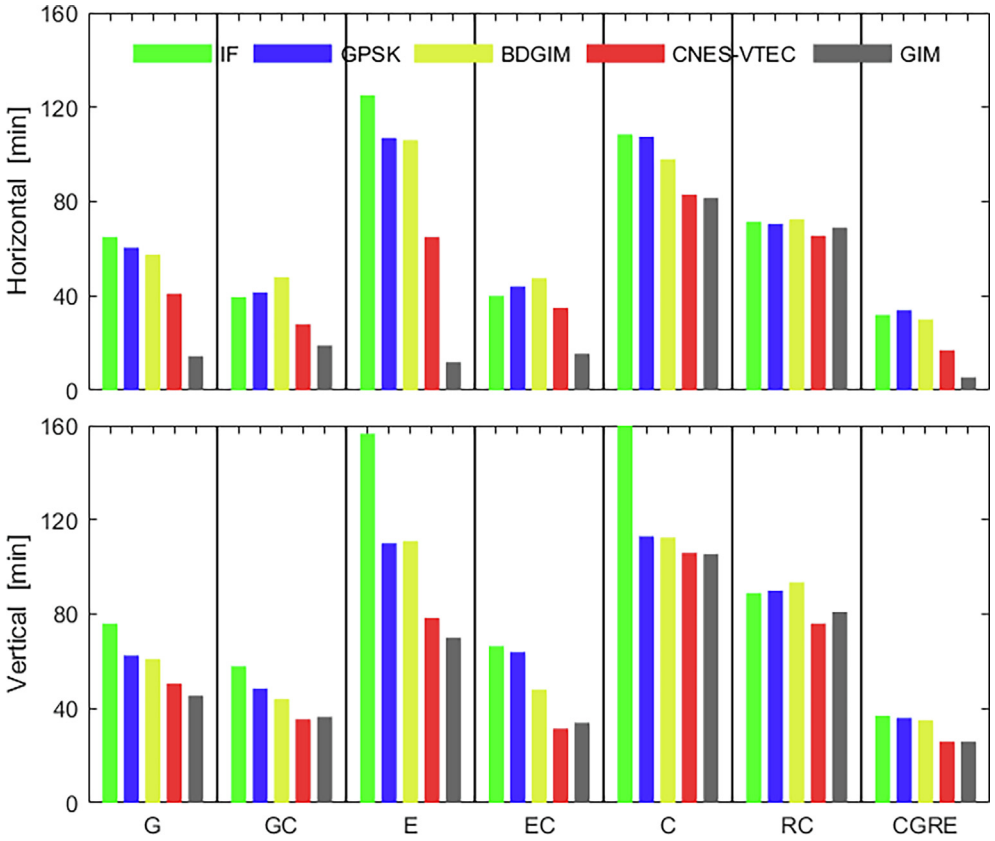

Fig. 10. Average convergence time of IF/IW SF-PPP in kinematic mode when the positioning errors converge to 0.3 m (27 MGEX stations, DoY 218–224, 2022).

Table 4
Improvement rates of the converge time for different IW solutions compared to the IF solutions (unit: %).

Component	System	GPS Klobuchar	BDGIM	CNES-VTEC	GIM
Horizontal	G	6.9	11.5	36.9	77.7
	GC	−5.1	−21.5	29.1	51.9
	E	14.4	15.2	48.0	90.4
	EC	−10.0	−18.8	12.5	61.3
	C	0.9	9.7	23.5	24.9
	RC	1.4	−1.4	8.4	3.5
	CGRE	−6.3	6.2	46.9	82.8
Vertical	G	17.8	19.7	33.6	40.1
	GC	16.4	24.1	38.8	37.1
	E	29.7	29.1	49.8	55.3
	EC	3.8	27.8	52.6	48.9
	C	37.2	37.5	41.1	41.4
	RC	−1.1	−5.1	14.6	9.0
	CGRE	2.7	5.4	29.7	29.7

shorter than that of both GPS Klobuchar- and BDGIM-constrained SF-PPP. In CNES-VTEC-constrained SF-PPP, the BDS-3 observations are more helpful to reduce the average convergence time of the Galileo-only solution compared to the GPS-only solution. Compared with the quad-system IF SF-PPP, the convergence time of CNES-VTEC-constrained SF-PPP has been greatly improved, with improvements of 46.9 and 29.7 % in the horizontal and vertical components, respectively. As to BDGIM-constrained SF-PPP, when the BDS-3 observations are integrated into the GPS/Galileo-only solutions, their convergence time can be reduced by up to 55.2 % in horizontal and 56.8 % in vertical. Note that the horizontal convergence time of the BDGIM-constrained solution in GPS + BDS-3, Galileo + BDS-3 and GLONASS + BDS-3 SF-PPP is even longer than that of IF SF-PPP. This phenomenon illustrates the BDGIM constraint has a negative impact on the horizontal convergence of the IW SF-PPP. On the other hand, when integrating the GLONASS observations in the BDGIM-constrained solution, the convergence time of the multi-GNSS SF-PPP could be increased, which is caused by the strong correlation of the IFCB and ionospheric parameters. With regard to the quad-system solutions, compared with the IF SF-PPP, the improvement of convergence time for BDGIM-constrained SF-PPP is relatively limited, with only 6.2 % in horizontal and 5.4 % in vertical. For the GPS Klobuchar-constrained solution, its convergence performance is similar to the BDGIM model, with improvements mainly reflected in the vertical component.

Table 5 summarizes the RMS of positioning errors of IF/IW SF-PPP in kinematic mode for all selected stations during the testing period. The improvement rates of 3D positioning accuracy for multi-GNSS solutions in comparison with the single-GNSS solutions is given in Table 6. Except for the GPS Klobuchar-constrained solution, the positioning accuracy of all IW SF-PPP is better than that of the IF SF-PPP. This illustrates the GPS Klobuchar model with only 55 % ionospheric correction accuracy is not suitable for the IW solution. Compared with the IF SF-PPP, no matter what single-GNSS or multi-GNSS solutions, the proportion of improvement in positioning accuracy of BDGIM-, CNES-VTEC- and GIM-constrained SF-PPP increases in turn, especially in the vertical component. By integrating the BDS-3 observations,

Table 5
RMS of positioning errors of IF/IW SF-PPP after 2 h of convergence in kinematic mode (unit: m).

System	Solutions	N	E	U	2D	3D
G	IF	0.110	0.132	0.220	0.171	0.278
G	GPS Klo	0.118	0.138	0.237	0.182	0.306
G	BDGIM	0.108	0.125	0.222	0.162	0.277
G	CNES-VTEC	0.102	0.119	0.214	0.156	0.265
G	GIM	0.098	0.119	0.213	0.152	0.262
GC	IF	0.086	0.104	0.186	0.135	0.230
GC	GPS Klo	0.091	0.104	0.200	0.140	0.250
GC	BDGIM	0.086	0.093	0.189	0.124	0.227
GG	CNES-VTEC	0.077	0.084	0.169	0.113	0.203
GC	GIM	0.071	0.075	0.165	0.104	0.194
E	IF	0.132	0.211	0.252	0.245	0.352
E	GPS Klo	0.140	0.181	0.264	0.232	0.362
E	BDGIM	0.121	0.146	0.231	0.176	0.303
E	CNES-VTEC	0.110	0.143	0.213	0.179	0.278
E	GIM	0.095	0.124	0.201	0.156	0.254
EC	IF	0.086	0.126	0.192	0.152	0.244
EC	GPS Klo	0.082	0.102	0.193	0.136	0.240
EC	BDGIM	0.084	0.095	0.184	0.124	0.223
EC	CNES-VTEC	0.075	0.083	0.166	0.112	0.200
EC	GIM	0.067	0.075	0.157	0.101	0.187
C	IF	0.151	0.239	0.304	0.274	0.415
C	GPS Klo	0.160	0.215	0.301	0.279	0.419
C	BDGIM	0.142	0.189	0.282	0.229	0.366
C	CNES-VTEC	0.129	0.174	0.266	0.216	0.343
C	GIM	0.119	0.163	0.262	0.200	0.330
RC	IF	0.106	0.165	0.239	0.195	0.308
RC	GPS Klo	0.111	0.147	0.237	0.198	0.316
RC	BDGIM	0.117	0.140	0.234	0.185	0.298
RC	CNES-VTEC	0.114	0.149	0.233	0.187	0.299
RC	GIM	0.103	0.136	0.231	0.17	0.287
CGRE	IF	0.071	0.097	0.158	0.119	0.198
CGRE	GPS Klo	0.070	0.077	0.167	0.106	0.201
CGRE	BDGIM	0.070	0.076	0.160	0.103	0.190
CGRE	CNES-VTEC	0.061	0.066	0.144	0.090	0.170
CGRE	GIM	0.056	0.060	0.138	0.083	0.160

Table 6
Improvement rate of 3D positioning accuracy of IF/IW SF-PPP for the GNSS + BDS-3 solutions compared to single-GNSS solutions (unit: %).

Positioning solutions	G vs GC	E vs EC	C vs RC	C vs CGRE
Ionosphere-free	17.3	30.7	25.8	52.3
GPS Klo-constrained	18.3	33.7	24.6	52.0
BDGIM-constrained	18.1	26.4	18.6	48.1
CNES-VTEC-constrained	23.4	28.1	12.8	50.4
GIM-constrained	26.0	26.4	13.0	51.5

the 3D positioning accuracy of GPS-only IW SF-PPP based on the BDGIM, CNES-VTEC and GIM models can be improved by at least 18.1 %. It is noteworthy that the contribution of BDS-3 to Galileo in positioning accuracy is more than that of BDS-3 to GPS. Although the positioning accuracy of the BDS-3-only solution is not superior to both GPS-only and Galileo-only solutions, the dm-level positioning accuracy can be achieved in SF-PPP. If only the GLONASS observations are integrated into the BDS-3-only IW SF-PPP, the 3D positioning accuracy can be improved by no more than 18.6 % for different ionospheric models. Interestingly, the positioning accuracy of GLONASS + BDS-3 IW SF-PPP with different ionospheric models is at the same level and within 0.3 m. As expected, the BDS-3 + GPS + GLONASS + Galileo SF-PPP for both IF and IW models can achieve the best positioning accuracy in all multi-GNSS solutions. The positioning accuracy of quad-system IF SF-PPP can be less than 0.1 and 0.16 m in the horizontal and vertical components, respectively. The results of quad-system BDGIM-constrained SF-PPP in the vertical component are consistent with the above accuracy, but the horizontal positioning accuracy can be improved by 20 % to 0.08 m. Through the comprehensive assessment of the three widely used SF-PPP models (i.e., IC, IF and IW), the best kinematic positioning accuracy, with RMS values of 0.06 m in horizontal and 0.14 m in vertical, can be obtained from quad-system GIM-constrained SF-PPP.

5. Conclusions

In this contribution, three widely used SF-PPP models (i.e., IC, IF and IW) were tested using the observations of 27 global stations for 7 consecutive days. Meanwhile, the impact of the different ionospheric products (i.e., GPS Klobuchar, BDGIM, CNES-VTEC and GIM) on the performance of three SF-PPP models is mainly analyzed. Note that the influence of BDGIM model on the positioning results of IW SF-PPP is proposed for the first time, especially in terms of convergence. Some key findings are summarized as follows:

(1) Compared with the GPS/GLONASS/Galileo-only solutions in IC SF-PPP, the 3D positioning accuracy of GPS/GLONASS/Galileo + BDS-3 IC SF-PPP can be improved by 10.9/32.1/10.5 %, 7.4/35.5/6.9 %, 11.6/39.0/12.9 % and 11.2/41.0/11.9 % for the GPS Klobuchar, BDGIM, CENS-VTEC and GIM models, respectively. In dual-system IC SF-PPP, the contribution of BDS-3 to GLONASS in positioning accuracy is significantly better than that of BDS-3 to GPS/Galileo. When the quad-system observations are integrated into IC SF-PPP, it has the ability to achieve the best positioning accuracy, with the 3D RMS of 0.94, 0.70, 0.55 and 0.40 m for the GPS Klobuchar, BDGIM, CNES-VTEC and GIM models, respectively.
(2) With the integration of BDS-3 observations to GPS/Galileo-only IF SF-PPP, the convergence time can be shortened by 38.3 and 60.9 % in horizontal and 38.5 and 60.8 % in vertical, respectively. As for the 3D positioning accuracy, the improvements of 17.3 and 30.7 % can be obtained from the GPS + BDS-3 and Galileo + BDS-3 IF SF-PPP, respectively. As expected, the BDS-3 + GPS + GLONASS + Galileo IF SF-PPP has the best performance in all multi-GNSS solutions. Its 3D positioning accuracy can be less than 0.2 m and is 2–5 times better than that of quad-system IC SF-PPP using different ionospheric models.
(3) When it comes to the GIM-constrained SF-PPP, compared with the GPS/Galileo-only results, the improvements of 19.8/51.4 % for vertical convergence time can be achieved in the GPS/Galileo + BDS-3 solutions when converging to 0.3 m. While for horizontal convergence time, its values cannot be reduced by adopting the BDS-3 observations. In CNES-VTEC-constrained SF-PPP, the convergence time of GPS/Galielo + BDS-3 can be shortened by 31.7/46.2 % in horizontal and 29.7/59.9 % in vertical, respectively, compared with the GPS/Galileo-only solutions. As to BDGIM-constrained SF-PPP for GPS/Galileo-only, the convergence time of GPS/Galileo + BDS-3 solutions can also be improved, with improvements of 16.5/55.2 % in horizontal and 27.9/56.8 % in vertical. The GPS Klobuchar-constrained solution has a similar performance to the BDGIM model. For all BDS-3 + GPS + GLO NASS + Galileo IW SF-PPP solutions, the GIM-constrained model has the shortest convergence time with 5.5 in horizontal and 26.0 min in vertical, which is improved by 82.8 % and 29.7 % in the horizontal and vertical components, respectively, compared with the quad-system IF SF-PPP. While for the BDGIM-

constrained model, the improvement of convergence time is relatively limited, with only 6.3 % in horizontal and 5.4 % in vertical.

(4) By introducing the BDS-3 observations, the 3D positioning accuracy of GPS/Galileo-only IW SF-PPP based on the BDGIM, CNES-VTEC and GIM models can be improved by 18.1/26.4, 23.4/28.1 and 26.0/26.1 %, respectively. However, this improvement cannot be shown in the GPS Klobuchar-constrained solution. Importantly, the cm-level accuracy of 0.06 m for the horizontal positioning can be reached in quad-system GIM-constrained SF-PPP, which means that the multi-GNSS IW SF-PPP has the potential to be applied in more and more engineering and scientific applications in the future.

Data availability

The multi-GNSS observations are provided by the MGEX, which are available from the ftp://igs.ign.fr/pub/igs/data/campaign/mgex/daily/rinex3/yyyy/ddd/. The final precise satellite orbits and clocks are downloaded from the ftp://ftp.gfz-potsdam.de/pub/GNSS/products/mgex/. The DCB products are provided by the IGS analysis center (DLR) at the ftp://igs.ign.fr/pub/igs/products/mgex/dcb/%04d/. The GPS Klobuchar and BDGIM products are obtained from the broadcast ephemeris file (BRD4) at https://cddis.nasa.gov/archive/gnss/data/daily/%04d/%03d/22p/. The CNES-VTEC products are provided by the SSRA00CNE0XXX.22C file, which is generated from the CNES real-time service. The GIM products are provided by the IGS analysis center (CODE) at the https://cddis.nasa.gov/archive/gnss/products/ionex/%04d/%03d/.

CRediT Author Contribution Statement

A.W and Y.Z were involved in the conceptualization, formal analysis and methodology; Z.Z was involved in the data curation and investigation; A.W was involved in the writing - original draft; A.W, J.C, H.W and D.Y were involved in the funding acquisition and project administration. J.C and J.J were involved in the supervision. All authors were involved in the writing - review & editing.

Declaration of Competing Interest

The authors declare the following financial interests/personal relationships which may be considered as potential competing interests: [Ahao Wang reports financial support was provided by Fundamental Research Funds for the Central Universities. Ahao Wang reports financial support was provided by China Postdoctoral Science Foundation. Hu Wang reports financial support was provided by the National Natural Science Foundation of China. Debao Yuan reports financial support was provided by the National Natural Science Foundation of China. Junping Chen reports financial support was provided by Program of Shanghai Academic Research Leader.]

Acknowledgements

The authors would like to thank the GFZ for the provision of final precise satellite orbits and clocks data. We also sincerely thank the IGS, CNES and CODE for the provision of MGEX observations, DCB, GPS Klobuchar, BDGIM, CNES-VTEC and GIM products. This research was funded by the Fundamental Research Funds for the Central Universities (No. 2022XJDC05); China Postdoctoral Science Foundation (No. 2022M723404); the National Natural Science Foundation of China (No. 42274044, 52174160); the Program of Shanghai Academic/Technology Research Leader (No. 20XD1404500); the Innovation Training Program for College Students at China University of Mining and Technology-Beijing (No. 202202037). We thank three anonymous reviewers for their insightful comments and suggestions to improve our manuscript.

References

Boehm, J., Moller, G., Schindelegger, M., Pain, G., Weber, R., 2015. Development of an improved empirical model for slant delays in the troposphere (GPT2w). GPS Solut. 19, 433–441.

Chen, J., Zhang, Y., Yu, C., Wang, A., Song, Z., Zhou, J., 2022. Models and performance of SBAS and PPP of BDS. Satellite Navigat. 3, 4.

Feltens, J., 2003. The activities of the ionosphere working group of the International GPS Service (IGS). GPS Solut. 7 (1), 41–46.

Ghoddousi-Fard, R., Lahaye, F., 2016. Evaluation of single frequency GPS precise point positioning assisted with external ionosphere sources. Adv. Space Res. 57 (10), 2154–2166.

Gill, M., Bisnath, S., Aggrey, J., Seepersad, G., 2017. Precise Point Positioning (PPP) using Low-Cost and Ultra-Low-Cost GNSS Receivers. Proc. ION GNSS+ 2017, Institute of Navigation, Portland, Oregon, USA, September 25–29, 226–236.

Hernández-Pajares, M., Juan, J.M., Sanz, J., Qrus, R., Garcia-Rigo, A., Feltens, J., Komjathy, A., Schaer, S.C., Krankowski, A., 2009. The IGS VTEC maps: a reliable source of ionospheric information since 1998. J. Geod. 83 (3–4), 263–275.

Klobuchar, J.A., 1987. Ionospheric time-delay algorithm for single-frequency GPS users. IEEE Trans. Aerosp. Electron. Syst. 23, 325–331.

Li, B., Zang, N., Ge, H., Shen, Y., 2019. Single-frequency PPP models: analytical and numerical comparison. J. Geod. 93 (12), 2499–2514.

Liu, T., Yuan, Y., Zhang, B., Wang, N., Tan, B., Chen, Y., 2017. Multi-GNSS precise point positioning (MGPPP) using raw observations. J. Geod. 91, 253–268.

Lou, Y., Zheng, F., Gu, S., Wang, C., Guo, H., Feng, Y., 2016. Multi-GNSS precise point positioning with raw single-frequency and dual-frequency measurement models. GPS Solut. 20 (4), 849–862.

Montenbruck, O., 2003. Kinematic GPS positioning of LEO satellites using ionosphere-free single frequency measurements. Aerosp. Sci. Technol. 7, 396–405.

Montenbruck, O., Hauschild, A., Steigenberger, P., 2014. Differential code bias estimation using multi-GNSS observations and global ionosphere maps. Navigation – J. ION 61 (3), 191–201.

Nie, Z., Yang, H., Zhou, P., Gao, Y., Wang, Z., 2019. Quality assessment of CNES real-time ionospheric products. GPS Solut. 23, 11.

Odolinski, R., Teunissen, P.J.G., 2018. An assessment of smartphone and low-cost multi-GNSS single-frequency RTK positioning for low, medium and high ionospheric disturbance periods. J. Geod. 93 (5), 701–722.

Orus, R., Hernandez-Pajares, M., Juan, J.M., Sanz, J., Garcıa-Fernandez, M., 2002. Performance of different TEC models to provide GPS ionospheric corrections. J. Atmos. Sol. Terr. Phys. 64 (18), 2055–2062.

Shi, C., Gu, S., Lou, Y., Ge, M., 2012. An improved approach to model ionospheric delays for single-frequency precise point positioning. Adv. Space Res. 49, 1698–1708.

Shi, C., Wu, X., Zheng, F., Wang, X., Wang, J., 2021. Modeling of BDS-2/BDS-3 single-frequency PPP with B1I and B1C signals and positioning performance analysis. Measurement 178 109355.

Su, K., Jin, S., Hoque, M.M., 2019. Evaluation of ionospheric delay effects on multi-GNSS positioning performance. Remote Sens. 11, 171.

Wang, A., Chen, J., Zhang, Y., Meng, L., Wang, J., 2019. Performance of Selected Ionospheric Models in Multi-Global Navigation Satellite System Single-Frequency Positioning over China. Remote Sens. 11, 2070.

Wang, A., Chen, J., Zhang, Y., Meng, L., Wang, B., Wang, J., 2020a. Evaluating the impact of CNES real-time ionospheric products on multi-GNSS single-frequency positioning using the IGS real-time service. Adv. Space Res. 66 (11), 2516–2527.

Wang, A., Chen, J., Zhang, Y., Wang, J., 2020b. Comparison of three widely used multi-GNSS real-time single-frequency precise point positioning models using the International GNSS Service real-time service. IET Radar Sonar Navig. 14 (11), 1726–1734.

Wang, S., Ge, Y., Meng, X., Shen, P., Wang, K., Ke, F., 2022b. Modelling and Assessment of Single-Frequency PPP Time Transfer with BDS-3 B1I and B1C Observations. Remote Sens. 14, 1146.

Wang, A., Zhang, Y., Chen, J., Wang, H., 2022a. Improving the (re-) convergence of multi-GNSS real-time precise point positioning through regional between-satellite single-differenced ionospheric augmentation. GPS Solut. 26 (2), 39.

Yuan, Y., Wang, N., Li, Z., Huo, X., 2019. The BeiDou global broadcast ionospheric delay correction model (BDGIM) and its preliminary performance evaluation results. Navigation 66 (1), 55–69.

Zhang, Y., Chen, J., Gong, X., Chen, Q., 2020. The update of BDS-2 TGD and its impact on positioning. Adv. Space Res. 65 (11), 2645–2661.

Zhang, H., Gao, Z., Ge, M., Niu, X., Huang, L., Tu, R., Li, X., 2013. On the convergence of ionospheric constrained precise point positioning (IC-PPP) based on undifferential uncombined raw GNSS observations. Sensors 13, 15708–15725.

Zhang, Q., Liu, X., Liu, Z., Hu, Z., Zhao, Q., 2022. Performance evaluation of BDS-3 ionospheric delay correction models (BDSK and BDGIM): First year for full operational capability of global service. Adv. Space Res. 70 (3), 687–698.

Zhou, F., Dong, D., Ge, M., Li, P., Wickert, J., Schuh, H., 2018. Simultaneous estimation of GLONASS pseudorange inter-frequency biases in precise point positioning using undifferenced and uncombined observations. GPS Solut. 22 (1), 19.

Zhou, F., Dong, D., Li, P., Li, X., Schuh, H., 2019. Influence of stochastic modeling for inter-system biases on multi-GNSS undifferenced and uncombined precise point positioning. GPS Solut. 23, 59.

Zhou, F., Cao, X., Ge, Y., Li, W., 2020. Assessment of the positioning performance and tropospheric delay retrieval with precise point positioning using products from different analysis centers. GPS Solut. 24, 12.